Chemico-Biological Interactions 387 (2024) 110813

Contents lists available at ScienceDirect

Chemico-Biological Interactions

journal homepage: www.elsevier.com/locate/chembioint

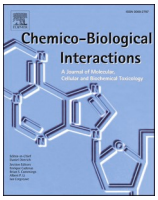

PODO/TERT256 – A promising human immortalized podocyte cell line and its potential use for *in vitro* research at different oxygen levels

Nadja Schlichenmaier, Alexander Zielinski, Sascha Beneke, Daniel R. Dietrich *

Human and Environmental Toxicology, Department of Biology, University of Konstanz, Konstanz, Germany

ARTICLE INFO

Keywords:
Kidney
Podocytes
Physiological oxygen

ABSTRACT

Podocytes are of key interest for the prediction of nephrotoxicity as they are especially sensitive to toxic insults due to their central role in the glomerular filtration apparatus. However, currently, prediction of nephrotoxicity in humans remains insufficiently reliable, thus highlighting the need for advanced *in vitro* model systems using human cells with improved prediction capacity. Recent approaches for refining *in vitro* model systems focus on closely replicating physiological conditions as observed under the *in vivo* situation typical of the respective nephron section of interest. PODO/TERT256, a human immortalized podocyte cell line, were employed in a semi-static transwell system to evaluate its potential use as a human podocyte *in vitro* system for modelling potential human glomerular toxicity. Furthermore, the impact of routinely employed excessive oxygen tension (21 % - AtmOx), when compared to the physiological oxygen tensions (10 % - PhysOx) observed *in vivo*, was analyzed. Generally, cultured PODO/TERT256 formed a stable, contact-inhibited monolayer with typical podocyte morphology (large cell body, apical microvilli, finger-like cytoplasmic projections (reminiscent of foot processes), and interdigitating cell-cell junctions) and developed a size-selective filtration barrier. PhysOx, however, induced a more pronounced *in vivo* like phenotype, comprised of significantly larger cell bodies, significantly enhanced filtration barrier size-selectivity, and a remarkable re-localization of nephrin to the cell membrane, thus suggesting an improved *in vitro* replication of *in vivo* characteristics. Preliminary toxicity characterization with the known glomerulotoxin doxorubicin (DOX) suggested an increasing change in filtration permeability, already at the lowest DOX concentrations tested (0.01 μM) under PhysOx, whereas obvious changes under AtmOx were observed as of 0.16 μM and higher with a near all or nothing effect. The latter findings suggested that PODO/TERT256 could serve as an *in vitro* human podocyte model for studying glomerulotoxicity, whereby culturing at PhyOx tension appeared critical for an improved *in vivo*-like phenotype and functionality. Moreover, PODO/TERT256 could be incorporated into advanced human glomerulus systems *in vitro*, recapitulating microfluidic conditions and multiple cell types (endothelial and mesenchymal cells) that can even better predict human glomerular toxicity.

1. Introduction

Mature podocytes are highly specialized, terminally differentiated cells that play a key role in glomerular filtration [1,2]. They wrap around the glomerular capillaries, thereby building a network of interdigitating foot processes (FP) that are connected via a specialized adherens junction called the slit diaphragm [3]. When the primary filtrate passes the slit diaphragm high molecular weight molecules such as plasma proteins are kept back, making the podocytes an essential component of glomerular filtration. At their basolateral side, podocytes are connected to the glomerular basement membrane via integrins and dystroglycans. The glomerular basement membrane itself is mainly made up of collagen type IV, laminin and proteoglycans, and is in direct contact with the fenestrated glomerular endothelium which completes the glomerular filtration barrier [4,5]. Accordingly, any pathological change in the glomerular filtration apparatus will have downstream effects on filtration rate, blood pressure, urine production, and retention of ions, glucose, amino acids and proteins as well as excretion of breakdown products e.g. urea and uric acid [6]. Indeed, glomerular diseases account for app. 90 % of end-stage renal disease in the US [7]

* Corresponding author.
E-mail addresses: nadja@schlichenmaier.net (N. Schlichenmaier), alexander.zielinski@uni-konstanz.de (A. Zielinski), sascha.beneke@uni-konstanz.de (S. Beneke), daniel.dietrich@uni-konstanz.de (D.R. Dietrich).

https://doi.org/10.1016/j.cbi.2023.110813
Received 18 September 2023; Received in revised form 7 November 2023; Accepted 9 November 2023
Available online 24 November 2023

and most glomerulopathies are characterized by podocyte injury, resulting in fibrosis, proteinuria and loss of kidney function [8–10]. As mature podocytes have a limited regenerative potential, podocytes are especially vulnerable to various toxic insults [11–13] within the functional setting of a complex glomerulus under physiologic conditions (blood filtration, blood pressure, etc.). In view of the latter, the robust, reproducible and sensitive assessment of human podocyte toxicity *in vitro* is key for understanding human glomerulopathies and prediction of glomerulotoxicity either for enhancing mechanistic understanding or for medium-high-throughput screening. As primary cells dedifferentiate quickly and are not readily available in sufficient quantities with reproducible quality, they are unsuitable for screening purposes as well as mechanistic studies [14]. Of the human podocyte cell lines generated [1,15–17] the temperature sensitive SV40 large T antigen immortalized human podocyte cell line (CIHP-1) [18] is the one that has been more broadly used [19–22], whereas conditionally immortalized podocytes isolated and cultured from human urine have proven more cumbersome and less robust [23]. However, conditionally immortalized human podocyte cell lines have also been criticized since some reports show phenotypic variations between and within cultures [24–26], as was shown for many other primary and cancer cells that were immortalized with a temperature sensitive SV40 large T antigen [27]. In view of the latter, a growing number of researchers focus on generating podocytes from induced pluripotent stem cells whereby several differentiation protocols have been established [28–33]. However, working with stem cells comes with its own caveats such as time-consuming differentiation, expensive media supplements, complex handling, and issues e.g. reproducibility, robustness and scaling that can hamper their applicability for mechanistic investigations and/or medium-large-scale drug screening. In contrast to the latter, current *in vitro* nephrotoxicity tests have not been able to replace *in vivo* animal tests, despite the awareness of the limited translatability of animal tests to the human situation, i.e. resulting in a predictivity of human nephrotoxicity of at best 70 % [34,35]. Consequently, major efforts are under way to establish *in vitro* models that are able to correctly predict nephrotoxicity in humans [36,37]. One main caveat of *in vitro* models is that they rarely mimic the physiological and structural environment of cells, potentially leading to aberrant protein expression and thus tissue functionality compared to the respective situation *in vivo* [38]. Several efforts have been made to provide cells with a more physiological environment and include e.g. co-cultures to allow cell-cell interactions, three-dimensional scaffolds, organoids, and microfluidic systems that apply shear stress [30,39–41]. All these factors have been shown to positively influence *in vitro* performance of cells. However, one factor that is generally ignored in nearly all *in vitro* approaches carried out today is proper oxygen tension. Standard routine cell cultures and procedures are nearly all carried out at atmospheric oxygen (AtmOx – app. 18–20 % O_2 in the media) while in contrast to the true *in vivo* situation, in blood of the renal cortex only approximately 10 % O_2 (PhysOx) are consistently reported [42,43]. As it has been shown that AtmOx negatively influences both stem cells (loss of stemness) and primary cells (induction of growth inhibition) [44,45], it is plausible to assume that AtmOx could also hamper functionality of immortalized renal cells *in vitro* despite that they do not appear to exhibit growth inhibition [46]. Indeed, several studies have provided evidence that immortalized cells are negatively influenced by AtmOx e.g. due to elevated reactive oxygen species leading to oxidative stress, which in turn can lead to changes in epigenetic programming, cellular proteome and stress responses [38,47–49].

PODO/TERT256, a human podocyte cell line that had been immortalized by the overexpression of the catalytic subunit of human telomerase (hTERT), appeared a viable alternative to current approaches [21,22,28]. hTERT overexpression prevents the shortening of telomeres and had been shown to immortalize cells without inducing cancer-associated changes or altering the cellular phenotype [50]. While the characterization of the PODO/TERT256 cell line focused on phenotypic expression and functionality in order to determine whether it might be a suitable tool for future podocyte research, choosing an appropriate cell line is only the first step in developing an *in vitro* model system that enables testing for podotoxicity and finally glomerulotoxicity with the goal to mimic human *in vivo* glomerulotoxicity. For better comparison with routine AtmOx conditions PODO/TERT256 were cultured at AtmOx and PhysOx in order to determine whether a change in oxygen tension would provide for near *in vivo*-like phenotypic characteristics and functionality. PODO/TERT256 presented with a typical podocyte morphology and formed a stable contact inhibited monolayer that acted as a size-selective filtration barrier. Culturing cells at PhysOx led to changes in morphology e.g. larger cell bodies with distinct finger-like cytoplasmic projections (reminiscent of foot processes) and suggested a higher sensitivity to the glomerulotoxin Doxorubicin when tested via the filtration assay.

2. Materials and methods

2.1. Cell culture

PODO/TERT256 cells were obtained from Evercyte GmbH, Austria (Cat# CHT- 033-0256), who also generously provided the corresponding parental human primary podocytes comparison. PODO/TERT256 were cultured in a 1:1 mix of DMEM no glucose (Cat# 11,966,025, Thermo Fisher) and Ham's F12 nutrient mix (Cat# 11,765,054, Thermo Fisher) supplemented with ITS-G solution (Cat# 41,400,045, Thermo Fisher), 2 mM GlutaMax (Cat# 35,050,061, Thermo Fisher), 100 U/ml Penicillin/Streptomycin (Thermo Scientific) and 1 % FCS. Parental cells were cultured in EGM-MV BulletKit (Cat# CC-3125, Lonza) supplemented with 20 % FCS. All cell culture plastic was pre-coated with 50 μg/ml human collagen I (Cat# 5007, Cell Systems) in PBS for 30 min at 37 °C to facilitate cell attachment. If not indicated otherwise, PODO/TERT256 were seeded in 12-well PET transwell inserts with 0.4 μm pores (Sarstedt) at a density of 15,000 cells/cm^2. Cells were cultured either at standard condition (AtmOx: atmospheric oxygen ≈ 21 %, 5 % CO_2, 37 °C, 95 % humidity) or physiological conditions (PhysOx: 10 % oxygen, 5 % CO_2, 37 °C, 75 % humidity, SciTIV Baker Ruskinn Low-Ox chamber, medium equilibrated to atmosphere for 24 h) with medium renewal every second or third day. Cell culture supernatant was saved after every medium exchange and stored at 4 °C to be used for later analysis. Morphology was assessed by microscopy (AtmOx: ECLIPSE TS100/TS100-F, Nikon, PhysOx: EVOS M5000, Invitrogen). Cell numbers were measured using the Beckmann Coulter Z1 Particle Counter (AtmOx) or the Omni Life Science CASY Cell Counter (PhysOx).

2.2. LDH leakage

Leakage of lactate dehydrogenase (LDH) into the cell culture medium was analyzed enzymatically based on the reduction of NADH to NAD [51]. 30 μl of cell culture supernatant was mixed with 170 μl reaction mix containing 1.25 mM NADH and 3.1 mM sodium pyruvate in 25 mM potassium phosphate buffer (pH 7.5). Absorption of NADH was measured every minute over a period of 30 min using a microplate reader (M200Pro, Tecan) that had been preheated to 37 °C. The slope of the reaction during linear decrease corresponds to the amount of LDH leaked into the cell culture supernatant. Cells lysed in 0.1 % Triton-X 100 were used to quantify intracellular LDH activity. Percent of cell death (% LDH leakage) was calculated by dividing extracellular LDH activity by the sum of extracellular and intracellular activity.

2.3. Scanning electron microscopy

After cells were grown for 7 days the transwell membranes were cut out using a scalpel and cells were pre-fixed using a 1:1 mixture of media with fixative at 37 °C for 20 min while transported to the Electron Microscopy Center of the University of Konstanz. Briefly, two further fixation steps using pure fixative (3 % formaldehyde, 2 % glutaraldehyde,

0.09 M sucrose, 0.01 M $CaCl_2$ and 0.01 M $MgCl_2$, in 0.1 M HEPES pH 7.2) were performed [52]: at 4 °C for 6 h followed by 30 min at 4 °C. Post fixation, membranes were washed three times for 5 min at 4 °C with buffer I (0.09 M sucrose, 0.01 M $CaCl_2$ and 0.01 M $MgCl_2$, in 0.1 M HEPES pH 7.2) and subsequently treated with 1 % OsO_4 in dH2O for 60 min at 4 °C in the dark. Membranes were washed three times for 5 min at 4 °C with buffer II (0.01 M $CaCl_2$ and 0.01 M $MgCl_2$, in 0.1 M HEPES pH 7.2) followed by progressive dehydration in ethanol (at 4 °C: 30 %/7 min, 50 %/10 min, 70 %/10 min; at RT: 80 %, 90 %, 96 % and twice 100 % for 10 min each). Post dehydration samples were critical point dried over liquid CO_2 in a Leica EM CPD300 (Leica, Germany), glued to aluminium-stubs using carbon pads and sputter coated with 6 nm of platinum (Quorum Q150R, Quorum Technologies, UK) [53]. Imaging was done using a Zeiss Auriga FESEM (Zeiss, Germany). Images were adjusted for display using ImageJ [54].

2.4. Immunocytochemistry

Cells were grown for 7 days, washed with PBS, fixed with 4 % PFA for 30 min, permeabilized with 0.1 % Triton-X 100 for 10 min and blocked with 1 % BSA/TBS-T for 1 h at room temperature. The transwell membranes were cut out using a scalpel and incubated with primary antibody (rabbit anti-nephrin (Cat# ab136894, Abcam), 1:100; mouse anti-P-cadherin (Cat# sc-514,481, Santa Cruz), 1:50; mouse anti-podocalyxin (Cat# sc-23904, Santa Cruz), 1:50; rabbit anti-WT1 (Cat# HPA053848, Sigma), 1:50 in 1 % BSA/TBS-T) solution at 4 °C overnight. After washing three times with PBS, membranes were incubated with secondary antibody (goat anti-rabbit AlexaFluor647 (Cat# A-21244, LifeTechnology) 1:1000; rabbit anti-mouse AlexaFluor647 (Cat# A-21239, LifeTechnology) 1:1000; goat anti-mouse AlexaFluor 488 (Cat# ab150113, Abcam) 1:1000 in 1 % BSA/TBS-T) solution for 2 h at room temperature in the dark. Membranes were washed three times with PBS and, if applicable, incubated with Phalloidin iFluor488 (Cat# ab176753, Abcam, 1:1000 in 1 % BSA/TBS-T) solution for 1 h at room temperature in the dark, followed by three wash steps with PBS. Cell nuclei were counterstained with Hoechst 3342 for 10 min. Membranes were transferred onto glass slides, mounted using fluorescence mounting medium (Cat# S3023, Dako), covered with a glass coverslip and sealed with nail polish. Cells were imaged using a point laser scanning confocal microscope LSM 700 (Zeiss). Images were adjusted for display using ImageJ.

2.5. Quantitative real-time PCR

Total RNA of samples was isolated using the PeqGOLD Total RNA Kit (Cat# 12–6834, VWR) following manufacturer's instructions. Reverse transcription was performed using the qScript cDNA Synthesis Kit (Cat# 733–1175, VWR) following the manufacturer's instructions. Quantitative real-time PCR was performed in duplicates with 40 ng cDNA per sample in KAPA SYBR FAST Master Mix (2x) Universal (Cat# KK4601, Sigma) with 10 μM forward and reverse primer using the CFX Connect Real Time PCR Detection System (Bio-Rad) according to the protocol listed in Table S1. Primer sequences are listed in Table S2. Expression of target genes was normalized to the mean expression of two housekeeping genes (HPRT1 & RPL13A). Fold-change was calculated in relation to the parental cell line.

2.6. Glucose consumption

Cells were seeded at a density of approximately 14.000 cells per cm^2. Glucose consumption was analyzed enzymatically using the coupled reaction of glucose oxidase (GOD) and peroxidase (POD). 3.3 μl of cell culture supernatant was diluted with 6.6 μl 0.1 M sodium hydrogen phosphate and mixed with 90 μl reaction mix containing 100 U/ml GOD, 0.25 U/ml POD and 1.5 mg/ml 2.2-azino-bis-(3-ethylbenzothiazoline-6-sulfonic acid) (ABTS) in 0.1 M sodium hydrogen phosphate (pH 6.5). After an incubation of 40 min at room temperature absorption was measured at 420 nm using a microplate reader (Tecan). Amount of glucose was calculated using linear regression and a glucose standard curve (0–2 mM) and corrected for the dilution factor. Glucose consumption was calculated by subtracting the remaining glucose content in samples from the amount of glucose in fresh medium.

2.7. Lactate production

Lactate production was analyzed enzymatically as published by Limonciel et al. [55] without modification.

2.8. Transepithelial electrical resistance (TEER)

TEER was quantified manually using a Millicell-ERS (Millipore). Measurements were performed prior to medium exchange to ensure an undisturbed monolayer [56]. TEER was calculated by subtracting the background value of an empty transwell insert from all obtained values and multiplying the resulting values with the surface area of the measured inserts.

2.9. Filtration assay

For measuring the apparent permeability, 0.5 mg/ml of fluorescently labeled dextrans (FITC-Dextran, MW = 70 kDa (Cat# 90,718, Sigma); TRITC-Dextran, MW = 20 kDa (Cat#73766, Sigma) were added to the basolateral chamber and incubated at 37 °C and 5 % CO2. After 120, 180 & 240 min 50 μl were transferred from the upper well into a black half area plate and replenished with 50 μl fresh medium. Fluorescence was measured using a microplate reader (M200Pro, Tecan) at Ex = 493 nm/Em = 520 nm (FITC) and Ex = 550 nm/Em = 577 nm (TRIC). Amount of dextran was calculated using point-to-point regression and a dextran standard curve (0–0.6 mg/ml). The apparent permeability coefficient of the layer was calculated according to the following formula as published in Hubatsch et al. (2007):

$$apparent\ permeability(cm/sec) = \frac{V(ml)}{C_0\left(\frac{\mu g}{ml}\right)} * \frac{1}{A(cm^2)} * \frac{C_t\left(\frac{\mu g}{ml}\right)}{t(\mathrm{sec})}$$

V = volume receiving chamber
C_0 = initial concentration of dextran in donor chamber
A = surface area of the membrane
C_t = concentration of dextran in the receiving chamber
t = time of incubation

As there were no fluctuations in the apparent permeability coefficient at different measuring time-points all three measurements in one well were averaged.

3. Results

3.1. PODO/TERT256 formed a stable contact-inhibited monolayer

Podocytes in culture were generally characterized by a large irregularly shaped cell body, forming finger-like cytoplasmic projections and small processes (reminiscent of foot processes) (Figs. 1 and 2). As shown in Fig. 1, these cellular characteristics were observed irrespective of oxygen tension employed (Fig. 1A, left panels). Furthermore, analysis of LDH leakage demonstrated the absence of exacerbated cell death (Fig. 1B, Fig. S1C) at both PhysOx and AtmOx. Seven days in culture cells at both oxygen tensions appeared to form a confluent monolayer (Fig. 1A). However, cells at AtmOx had a significantly faster population doubling time than cells at PhysOx and continued to proliferate up to day 11, when they reached the plateau phase two days later than cells

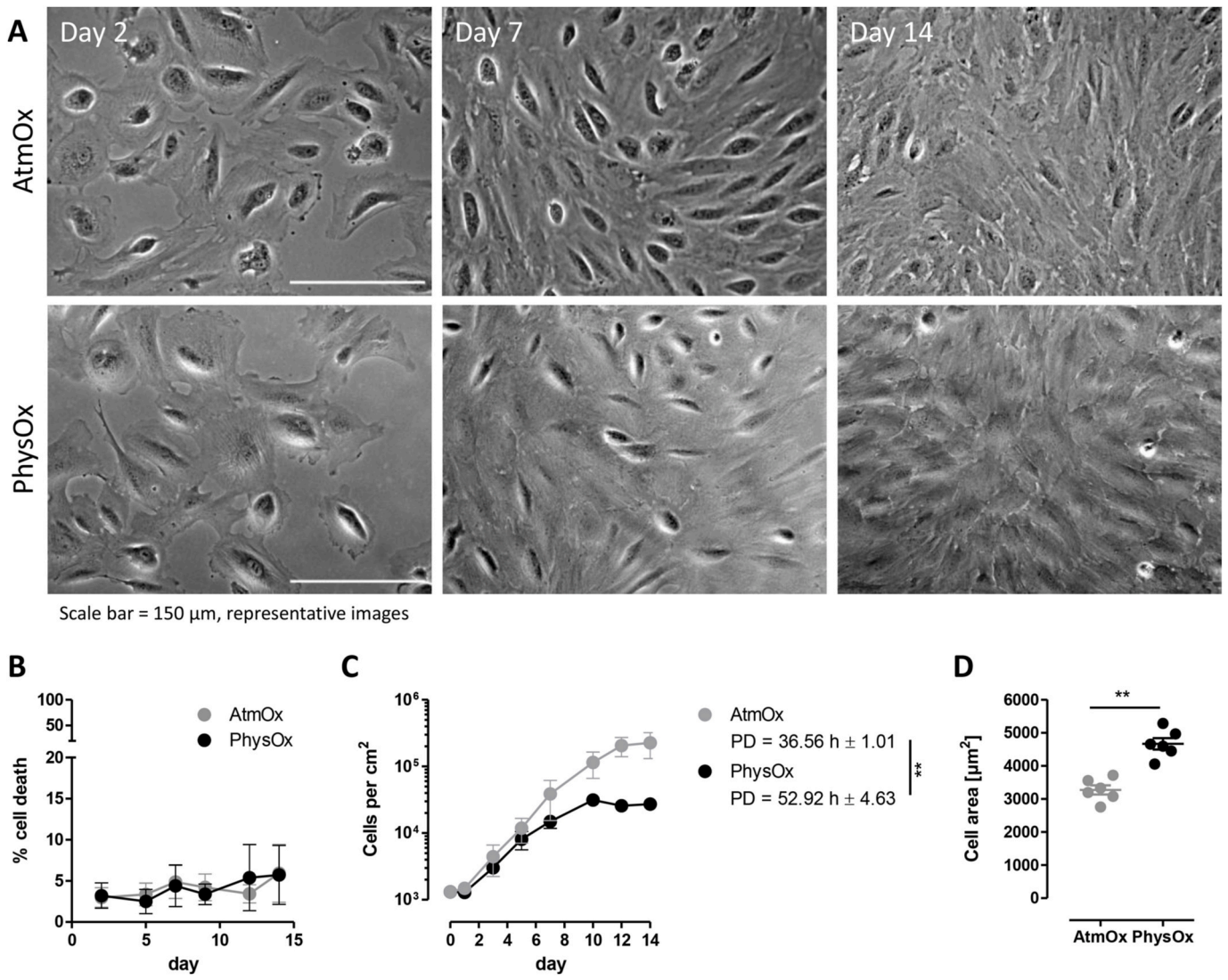

Fig. 1. Brightfield microscopic images, LDH release and cell growth in PODO/TERT256 routinely cultured at AtmOx and PhysOx **A** - Bright-field microscopy of PODO/TERT256 grown at AtmOx or PhysOx on normal cell culture plastic. Scale bar = 150 µm, representative images. **B** - LDH leakage revealed absence of exacerbated cell death for at least 14 days after seeding. n = 3, mean ± SEM. **C** - Cell proliferation over a period of 14 days after seeding. PD: Population doubling time, n = 3, mean ± SEM. p = 0.0022 (**), two-tailed *t*-test. **D** - Cell area on day 2 post seeding as calculated using ImageJ. n = 6, each dot represents the mean of 10 cells. Lines indicate mean ± SEM. p = 0.0022 (**), Mann-Whitney test.

grown at PhysOx. The resulting cell layer at AtmOx contained 8 times as many cells as the layer at PhysOx (Fig. 1C).

Despite the higher cell number at AtmOx, no overgrowth, multiple layering or dome formation was observed and cell numbers remained stable for up to 30 days (Fig. S1A and B). This suggested that the PODO/TERT256 cell layer was contact-inhibited, whereby cells entered a non-proliferative state upon reaching confluence. PODO/TERT256 cultured at PhysOx for 2 days had a significantly larger cell body, covering about 1.5 times the surface area (Fig. 1D) of podocytes cultures at AtmOx. The latter also supported the notion that the lower cell number at PhysOx was not the result of an adverse effect of the lower oxygen tension, but indicated that the larger body size could have resulted from low oxygen mediated differentiation processes.

3.2. PODO/TERT256 demonstrate typical podocyte morphology

Scanning electron microscopy (SEM) and immunocytochemistry (ICC) were used to further investigate and compare the phenotype of PODO/TERT256 at different oxygen levels. SEM images confirmed the typical podocyte morphology of PODO/TERT256 irrespective of oxygen tensions used. Cells were characterized by a large cell body covered by apical microvilli (Fig. 2A CB) and interconnected via interdigitating cell-cell junctions (Fig. 2A arrow). The cells formed small cytoplasmatic projections (filopodia [57]) occasionally branching into tertiary processes (Fig. 2A arrow head) reminiscent of main processes and FP known from podocytes *in vivo* [58]. ICC analysis confirmed expression of the podocyte marker proteins P-Cadherin, Podocalyxin, Nephrin & WT-1 in PODO/TERT256 (Fig. 2B). While WT-1, an important transcription factor, was correctly localized in the nucleus at both oxygen conditions [59], P-Cadherin and Nephrin, both part of the slit diaphragm [60], demonstrated an oxygen tension dependent distribution. While P-Cadherin was strongly localized at the cell membrane at AtmOx, PhysOx resulted in a more diffuse cellular distribution. In contrast, a more diffuse distribution was evident for Nephrin at AtmOx and a stronger localization to cell membrane was observed at PhysOx (Fig. 2B). In parental primary podocytes cultured for 7 days at PhysOx both Nephrin and P-Cadherin were mostly localized at the cell membrane with P-Cadherin also showing some cytosolic distribution (Fig. S2), thus suggesting that PODO/TERT256 at PhysOx displayed a Nephrin and P-Cadherin distribution comparable to the one observed in the parental

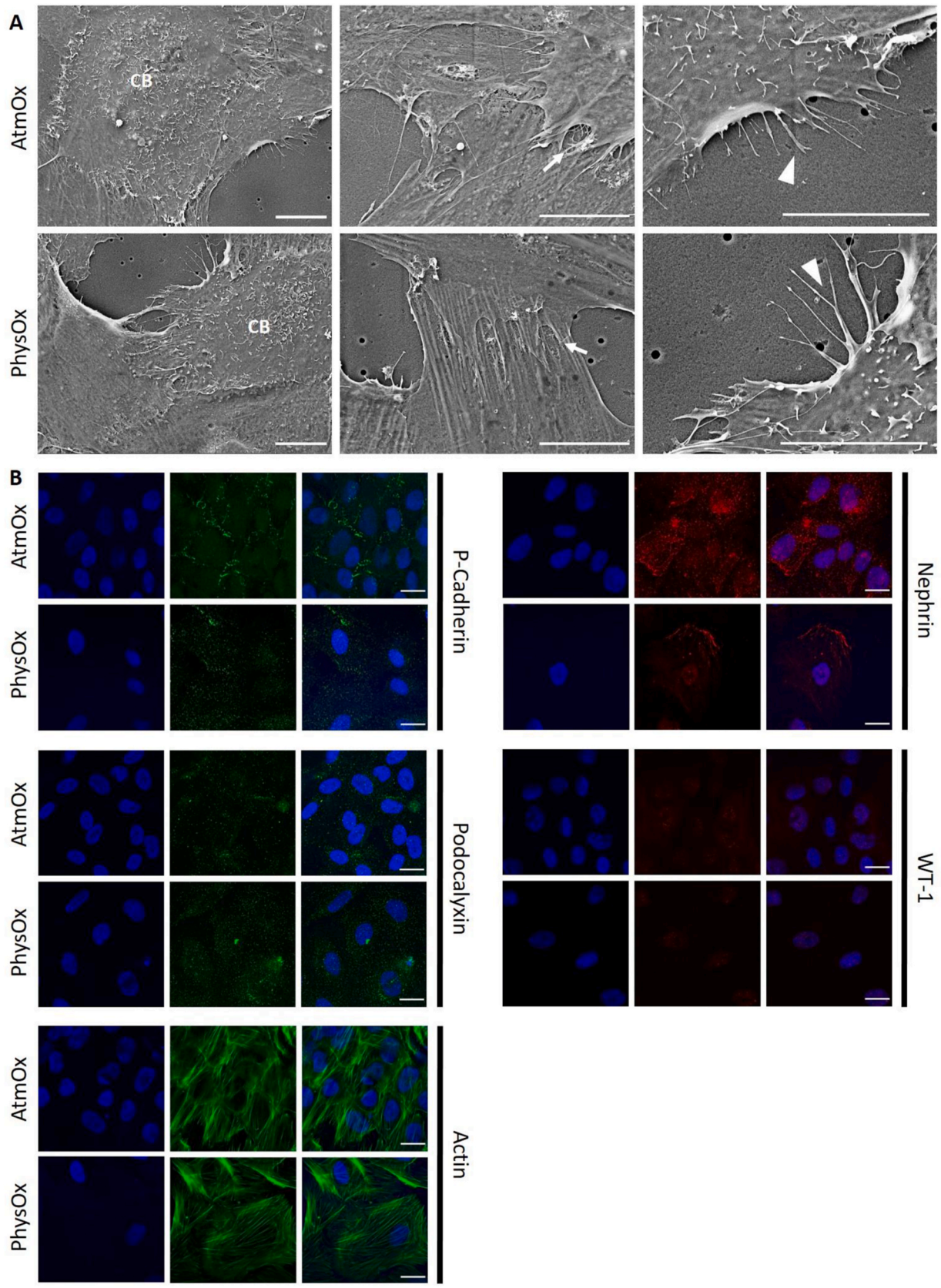

Fig. 2. SEM and ICC pictures of PODO/TERT256 cultured at AtmOx and PhysOx Cells were grown for seven days at AtmOx and PhysOx before imaging. **A** - SEM pictures demonstrated a large cell body (CB), interdigitating cell-cell junctions (arrow) and small tertiary projections (arrow head), reminiscent FP known from *in vivo* SEM illustrations [62]). Scale bar = 10 μm, representative images. **B**–ICC pictures demonstrating the expression and localization of P-Cadherin, Nephrin, Podocalyxin, WT-1 and Actin. Nuclei were counterstained with Hoechst. Scale bar = 20 μm, representative images.

primary podocytes cultured at physiological conditions and found *in vivo* [58]. Podocalyxin, being part of the podocyte glycocalyx and forming the base of microvilli in the apical membrane [61], presented with an even granular distribution within the cell body irrespective of the oxygen tensions and as also shown for the parental primary podocytes cultured at PhysOx (Fig. S2). The latter also applied to actin distribution, whereby phalloidin staining revealed a comparable actin cytoskeleton in PODO/TERT256 and parental primary podocytes irrespective of the oxygen tension, albeit larger cell bodies were observed at PhysOx, thus corroboration earlier observations (Fig. 1D).

3.3. PODO/TERT256 express a whole panel of podocyte marker genes

To further characterize PODO/TERT256, the expression level of a panel of genes important for podocyte functionality was analyzed. Included were genes encoding for slit diaphragm proteins (e.g. CDH3, NPHS1 & SYNPO), transmembrane receptors (e.g. ITGA3 and ITGB1), proteins of the glycocalyx (e.g. PODXL), and transporters (e.g. GLUT1 and 2) as listed in Fig. 3 (x-Axis).

Cells were grown for 2, 7 & 14 days prior to RNA isolation. Gene expression was analyzed using RT-qPCR and normalized to expression levels determined in the parental primary podocytes (dotted line). Data is shown as mean ± SEM, n = 3 biological replicates (with one exception with an n = 2). For statistical analysis a two-way ANOVA followed by a Bonferroni multiple comparisons test was performed with an n = 3 and an n = 2 for all datasets was performed with an n = 3 and an n = 2 for all datasets, without resulting in any observable differences in results obtained (F-values see Supplement Tables S3 and S4, $p \leq 0.0001$ = ****.

When compared to the parental primary podocytes cultured at PhysOx, all genes analyzed, with the exception of NPHS2 (podocin), were found to be expressed in PODO/TERT256. However, podocin mRNA was found expressed at very low levels in parental primary podocytes (data not shown). Most of the genes analyzed were expressed at comparable levels in PODO/TERT256 and the parental primary podocytes with the notable exceptions of PODXL and CDH3 being strongly upregulated and KIRREL2, ITGB1 and GLUT2 being slightly downregulated. In summary PODO/TERT256 showed a gene expression pattern typical for primary human podocytes *in vitro*. The gene expression pattern was comparable irrespective of culture duration (for up to 30 days see Fig. S3) and oxygen tensions. The only significant differences between PhysOx and AtmOx observed was an upregulation of CDH3 and ITGB1 (only at day 2) at PhysOx, albeit the observed differences appeared relatively small and thus could well have been observed by chance without any underlying biological meaning.

PODO/TERT256 form a size-selective filtration barrier.

A central function of podocytes *in vivo* is the establishment of a filtration barrier that enables size and charge selective filtration of molecules across the glomerular filtration barrier (GFB). To test whether PODO/TERT256 would form such a barrier *in vitro* the permeability of the layer to 20 and 70 kDa dextrans was tested and the respective permeability coefficient P_{app} calculated. A size-selective filtration barrier was formed by confluent PODO/TERT256 at AtmOx and PhysOx, allowing for facilitated movement of 20 kDa dextrans. However, it is to be noted that commensurate with the slower growth of podocytes under PhysOx (Fig. 1C), a slightly higher permeability to 20 and 70 kDa dextrans was observed on day 2 after seeding only (Fig. 4A), whereas cells then started to increase in body size and spread (Fig. 1D) which resulted in a lower permeability at day 7 and 14 under PhysOx (Fig. 4A) and thus a significantly higher filtration barrier i.e. 20/70 kDa ratio overall (Fig. 4B). The latter ratio remained unchanged over time (for up to day 30, see Fig. S4A) suggesting that the established filtration barrier remained stable. Corroboration of the latter was obtained by demonstrating a continuously stable transepithelial electrical resistance (TEER) of the confluent PODO/TERT256 of approximately 18 Ω*cm^2 irrespective of oxygen tension or culturing duration (Fig. 4C and Fig. S4B). A TEER of 18 Ω*cm^2 is testimony of a rather permeable barrier that allows water and smaller molecules <20 kD to pass nearly uninhibited, whereas very tight barriers (approximately 130 Ω*cm^2) e.g. formed by renal proximal tubule epithelial cells (RPTEC/TERT1), require tight junctions to reduce para-cellular transport and specific transporters for trans-cellular transport [63].

3.4. PODO/TERT256 glycolytic rate

Glucose is consumed to generate ATP via mitochondrial oxidative phosphorylation and/or glycoloysis to produce lactate. As podocyte FP appear devoid of mitochondria, all cytoskeletal rearrangements (e.g. actin, synpo) and signal transduction processes (e.g. nephrin-Nck-N-WASP pathway) requiring ATP [58] rely primarily on glycolysis. In contrast, the main cell body of podocytes can carry out mitochondrial oxidative phosphorylation. Thus, changes in oxygen tension should affect ATP production in the main cell body and FP differently. In order to develop a first impression on the effects of differences in oxygen tension on the ATP production, glucose consumption, lactate production and the glycolytic rate (lactate to glucose ratio) were determined in PODO/TERT256 at AtmOx and PhyOx conditions. The comparison of the glycolytic rate (Fig. 4D) demonstrated that while podocytes under AtmOx maintained a relatively stable glycolytic rate of approx. 1.0, cells at PhyOx demonstrated also a ratio of approx. 1.0 yet in conjunction with a much higher variability of the 14 days observation period. More in-depth analyses demonstrated that podocytes under AtmOx maintained the glycolytic ratio of approx. 1.0 throughout the days of

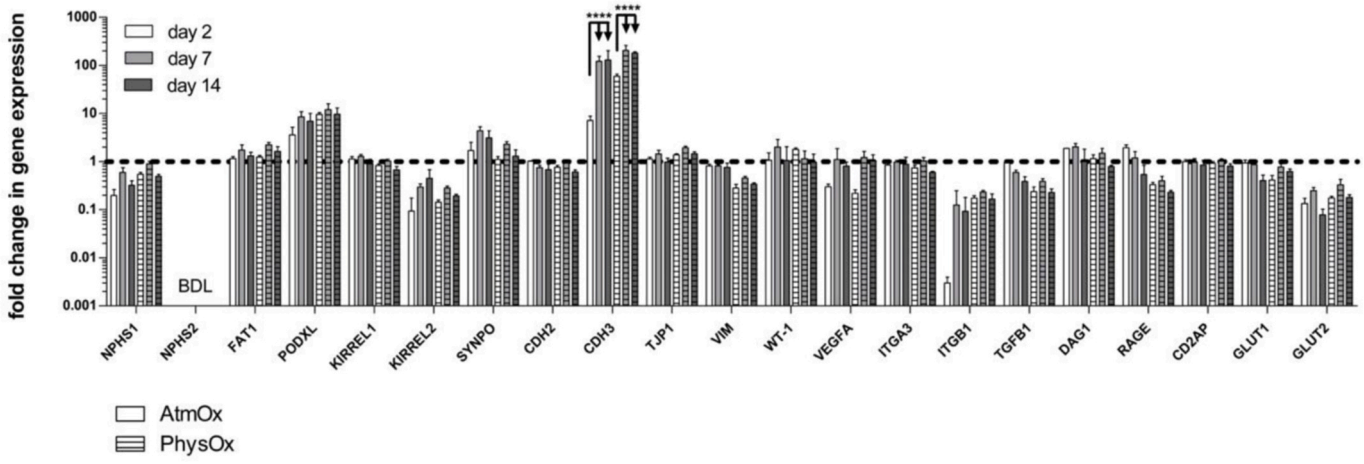

Fig. 3. RT-qPCR analysis of a panel of podocyte genes in PODO/TERT256 at AtmOx and PhysOx.

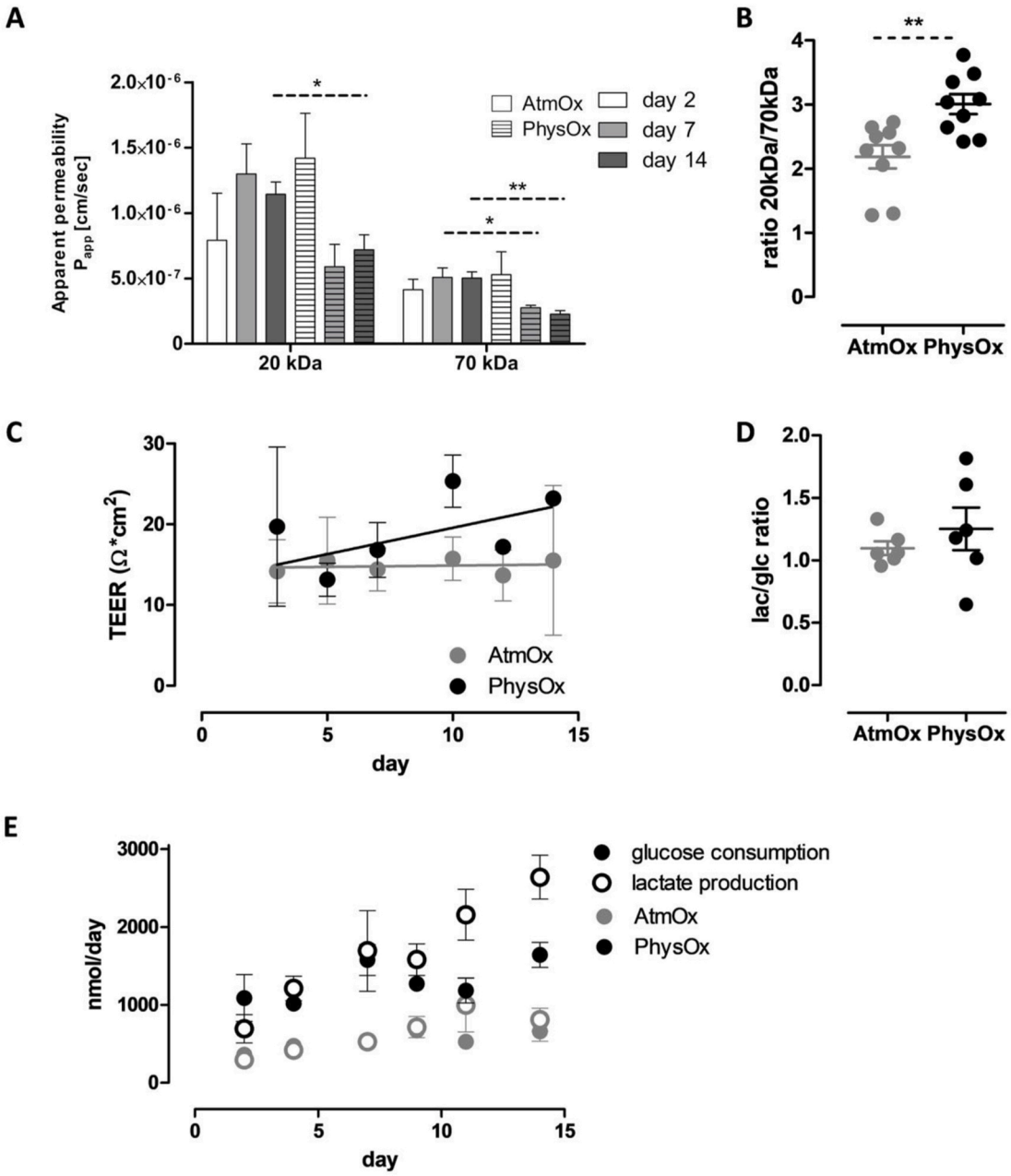

Fig. 4. Apparent permeability, transepithelial electrical resistance and glycolytic rate in PODO/TERT256 at AtmOx and PhysOx **A** – Permeability coefficients for two fluorescently labeled dextrans (20 and 70 kDa). Mean ± SEM, n = 3. For statistical analysis a two-tailed unpaired *t*-test between the two different oxygen tensions (*, dashed lines), *p < 0.05, and **p < 0.01. **B** – Cells at PhysOx established an improved size-selective filtration barrier as demonstrated by the significantly higher 20/70 kDa ratio. Each dot represents one replicate at one time point. Lines indicate mean ± SEM. p = 0.0035 (**), two-tailed unpaired *t*-test. **C** – Transepithelial electrical resistance (TEER) was stable for a minimum of 14 days after seeding. Mean ± SEM, n = 3. A linear regression analysis (ANCOVA) was carried out to allow for statistical analyses that demonstrated no significant differences. **D** - Glycolytic rate (as calculated by the ratio of lactate production and glucose consumption) over a period of 14 days after seeding. Each dot represents the mean of three biological replicates per timepoint. **E** – Glucose consumption (filled circles) and lactate production (empty circles) were measured enzymatically over a period of 14 days after seeding.

observation (Fig. 4E), thus corroborating that high oxygen tension favored oxidative phosphorylation where any aerobic glycolysis occurring would shunt pyruvate into the mitochondrial oxidative phosphorylation mechanism. In contrast, podocytes cultures at PhysOx started with high mitochondrial oxidative phosphorylation, as demonstrated by the low glycolytic ratio of approx. 1.0, which then, as cells grew to confluence and developed a demonstrable filtration barrier (Fig. 4 B), increased to a ratio of 1.5–2.0, suggesting high aerobic glycolytic activity (Fig. 4E) as would be expected from the active FP and the larger cell rea observed under PhysOx (Fig. 1D).

3.5. PODO/TERT256 are sensitive to the known glomerulotoxin doxorubicin (DOX)

In order to determine whether PODO/TERT256 are sufficiently sensitive to a model nephrotoxicant in *vitro* and what effect, if any, oxygen tension would have on the direction and intensity of the response, cells were treated with doxorubicin (DOX), a chemotherapeutic drug known to cause glomerulotoxicity in humans. Cells treated with concentrations ranging between 0.01 and 2.0 μM DOX demonstrated an apparently different concentration response to AtmOx and PhysOx, as determined via the permeability to 20 and 70 kD dextrans (Fig. 5A).

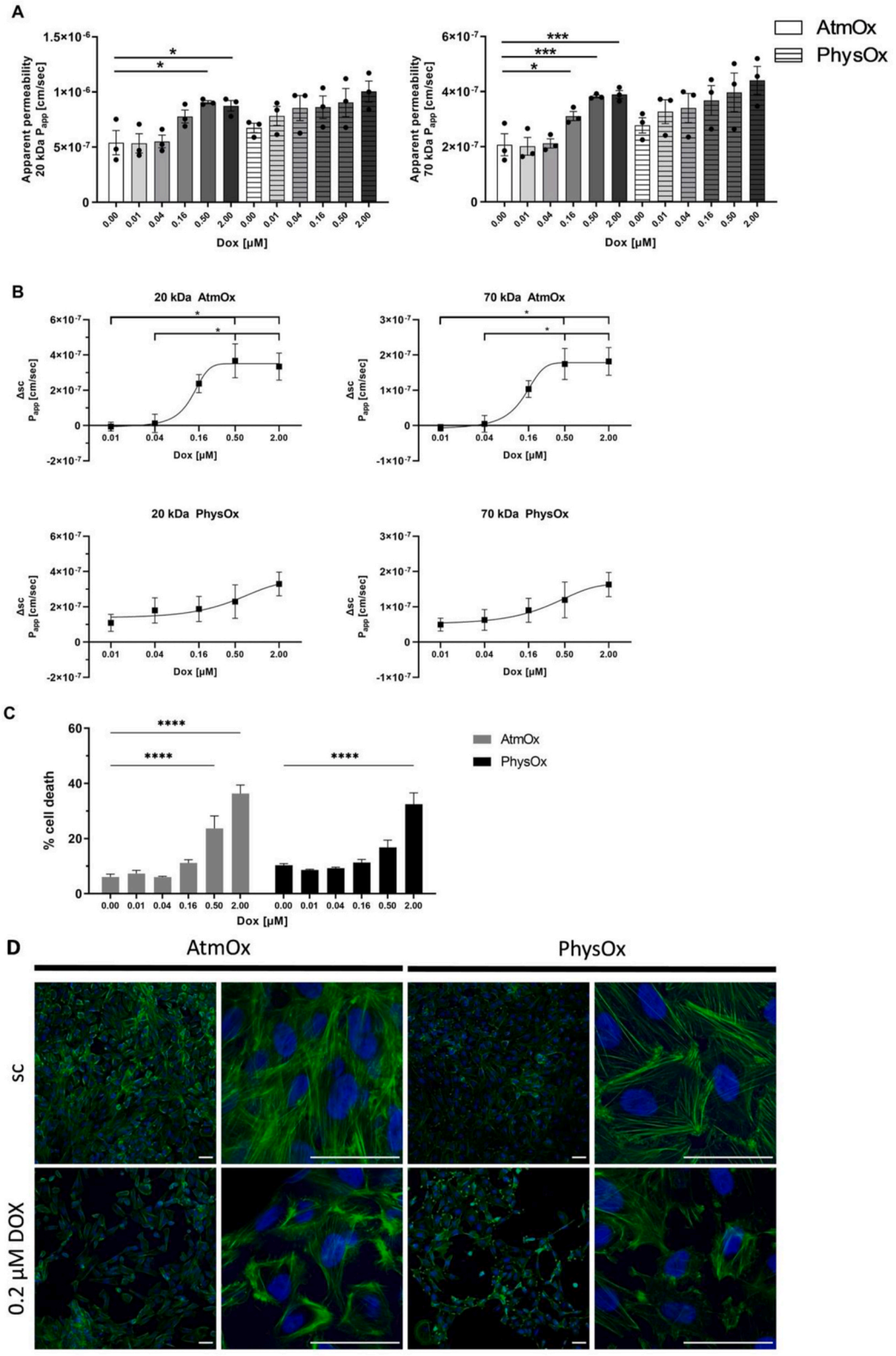

Fig. 5. Response of PODO/TERT256 to treatment with the known glomerulotoxin doxorubicin (DOX) at AtmOx and PhysOx Cells were grown for 7 days at AtmOx and PhysOx before treatment with DOX for 72 h. **A** – Apparent permeability coefficients for two fluorescently labeled dextrans (20 & 70 kDa). **B** – Treatment with DOX disturbs the filtration barrier and leads to a gradual increase of dextran diffusion at PhysOx, while evoking a late but sudden increase at AtmOx. The line represents non-linear curve fitting for a sigmoidal shaped curve. **C** – Cell death as determined via LDH leakage in cells treated with DOX for 72 h. **D** – ICC pictures showing the actin cytoskeleton in cells treated with or without DOX. Scale bar = 50 µm, representative images. All data is shown as mean ± SEM, n = 3. A one-way ANOVA followed by a Dunnett's (**A**) or Tukey (**B**) test was performed for statistical testing of permeability data, while a one-way ANOVA followed by a Dunnett's test was performed for cell death measurements (**C**). Significant differences: * = $p \leq 0.05$; ** = $p \leq 0.01$; *** = $p \leq 0.001$; **** = $p \leq 0.001$.

Indeed, while cells cultures at AtmOx presented with no change up to and including 0.04 μM DOX, higher concentrations of DOX increased permeability, albeit only the 0.5 and 2.0 μM values were significantly different from the control. Moreover, the concentration response curve appeared to describe an all or nothing response, whereas at 0.5 and 2.0 μM the maximum "leakiness" was already reached. In contrast, cells cultured at PhysOx generally appear more "leaky" at all DOX concentration employed, whereby the concentration-permeability curve followed a sigmoidal curve with the maximum "leakiness" presumably not yet reached at 2.0 μM (Fig. 5A and B). It has to be noted, however that permeability differences between the individual concentrations of DOX and control were not statistically significant due to the high variability between replicates encountered. Indeed, normalization to the control and reanalysis (Fig. 5B) confirmed the "steep" concentration response curve" of DOX for cells at AtmOx, whereas cells cultured at PhysOx appeared to respond with increased leakiness at all concentrations of DOX, i.e. even at the lowest concentration of 0.01 μM DOX employed. Cell death increased as of 0.5 μM DOX to reach the maximum at 2.0 μM, commensurate with increased permeability of cells under AtmOx (Fig. 5C). In contrast, significantly increased cell death under PhysOx was observed at the highest DOX concentration (2.0 μM) only, with a slight albeit not significant increase at 0.5 μM. The latter finding suggested that cell death was the primary driver for the increased permeability in PODO/TERT256 exposed to DOX at AtmOx, while increased permeability was observed already at the lowest concentrations of DOX independent of cell death at PhysOx (Fig. 5C). The latter suggesting that cytoskeletal changes rather than overt cytotoxicity as the driver for the increased permeability. Indeed, marked changes in cytoskeletal structure resulting in loss of cell-cell connections were observed for actin at 0.2 μM DOX at PhysOx (Fig. 5D), while no such changes were observed at AtmOx. The latter changes involved the relocalization of actin towards the cytoplasmic membrane, loss of cell-cell contacts and general rounding and shrinkage of cells. Similar rearrangements have been detected in ciPTECs treated with doxorubicin [64,65].

4. Discussion

Injury to podocytes inevitably leads to impairment of glomerular filtration, resulting in proteinuria, fibrosis and can ultimately lead to renal failure. Chronic kidney disease and end-stage renal failure are serious concerns in world-wide healthcare, creating both a huge economic burden and ever-increasing mortality rates [66–68]. Since it has been found that app. 90 % of cases of end-stage renal disease (ESRD) are directly linked to loss of glomerular function research has heavily focused on studying podocytes as the root cause of most glomerulopathies [6–10]. Podocytes are terminally differentiated cells with limited regenerative potential, making the glomerulus especially sensitive to toxic insults [13] and indeed, it has been estimated that 30–50 % of cases of ESRD are drug-induced [69]. Therefore, it is especially important to prevent nephrotoxic drugs from entering the market. Unfortunately, current pre-clinical tests are often unable to predict nephrotoxicity mostly due to species specific differences between test animals and humans [34,35]. This observation has driven research towards cell-based *in vitro* models [37]. For the success of such models, it is especially important to choose the right cells. These cells should be easy to handle and produce robust and reproducible read-outs [70], but also retain as many features of their *in vivo* counterparts as possible to allow high predictivity. In the case of podocytes primary cells are of little use, since they do not proliferate and dedifferentiate quickly *in vitro* [14]. To overcome this, researchers can either work with immortalized cells or cells generated from induced pluripotent stem cells [28,29]. In contrast to induced pluripotent stem cells that have been shown to provide for a reliable, albeit not easily transferable test system [28], PODO/TERT256 are a human derived podocyte cell line immortalized via telomerase overexpression. These cells are easy to handle since they proliferate continuously but stop when reaching confluence, displaying contact-inhibition (Fig. 1 A). In contrast to widely used conditionally immortalized cells [18] (in the following called ciPODs), these cells can continuously be kept at 37 °C, and there is no time-consuming differentiation protocol needed as is required for induced pluripotent stem cells [28]. Morphologically, PODO/TERT256 are comparable to differentiated ciPODs and podocytes derived from induced pluripotent stem cells following protocols by Song et al. Rauch et al., Bejoy et al. and Musah et al. [29,31–33]. PODO/TERT256 display a large cell body with cytoplasmatic projections and interdigitating connections between cells (Figs. 1 & 2A). Furthermore, these cells express a panel of podocyte marker genes at comparable levels to the parental primary cells (Fig. 3) with the exception of P-Cadherin, which is strongly upregulated in PODO/TERT256, and podocin, which is not expressed in PODO/-TERT256. However, podocin is also barely detectable in the parental cells. This might indicate that podocin expression was already lost during isolation and culturing of primary cells. Of note, both ciPODs and podocytes differentiated from pluripotent stem cells have demonstrated podocin expression [18,29,31–33]. The analysis of four podocyte-specific markers from different cell compartments (Podocalyxin – apical membrane, P-Cadherin & Nephrin – cell-cell contacts/slit diaphragm & WT-1 – nucleus) at the protein level, as suggested by Krtil et al. [15], confirmed their expression in PODO/TERT256 (Fig. 2B). Whereas functional parameters e.g. formation of a confluent cell layer, very low levels of cell death for up to 30 days (Fig. S1C), and the development of a size-selective filtration barrier (Fig. 4A and B), which was stable for up to 30 days (Fig. S4A), confirmed that PODO/TERT256 fulfilled all criteria required of human derived cells that can be robustly employed as an *in vitro* podocyte model.

However, as noted earlier, an appropriate cell line alone will not provide a truly more *predictive in vitro* alternative to *in vivo* tests in preclinical testing as long as testing is carried out under non-physiological conditions. Hence adjusting culturing conditions of PODO/TERT256 to the physiologically normal 10 % oxygen tension (PhysOx) resulted in the formation of a stable contact-inhibited monolayer with typical podocyte morphology, albeit with a slower doubling time, but a significantly larger cell body (Figs. 1 & 2B). Indeed, PODO/TERT256 at PhysOx increased in size up to a length of 150 μm similarly to what has been reported in differentiated ciPODs [71]. As PhyOx conditions may also impact basic metabolism and ATP generation and the latter often can play a key role in the molecular events resulting in cell toxicity [72], the ratio of glucose consumption and lactate production was determined as an estimate of glycolytic rate. Indeed, as podocyte FP appear devoid of mitochondria, all cytoskeletal rearrangements (e.g. actin, synpo) and signal transduction processes (e.g. nephrin-Nck-N-WASP pathway) requiring ATP [58] rely primarily on glycolysis. Moreover, as changes in metabolism and thus reorganization of FPs will critically affect the function of the slit diaphragm, downstream effects of changes in podocyte and thus FP metabolism (Fig. 4) will affect filtration of the podocytes and thus permeability as shown in Fig. 5.

While Brinkkoetter et al. [73], using both *in vivo* experiments in mice and *in vitro* experiments on primary mice cells and ciPODs, suggested that podocytes primarily rely on anaerobic glycolysis to maintain cellular function, data generated in these experiments strongly suggested that PODO/TERT256 cultured at AtmOx primarily gained ATP via mitochondrial oxidative phosphorylation (OXPHOS), whereas cells maintained at PhysOx moved toward increased aerobic glycolysis (Fig. 4). Additional data generated (data not shown) using 2-deoxglucose, and thus inhibition of glycolysis, did not result in increased cell death or apoptosis at either oxygen tension. The latter, however, would appear to stand in contrast to the study by Ozawa et al. [74] using conditionally immortalized mouse podocytes that found that blocking glycolysis, but not OXPHOS, induced apoptosis and disturbed cell morphology. However, beyond the fact that mouse podocytes may react slightly differently to human podocytes, treatment of PODO/TERT256 with DOX resulted in increased permeability to 20/70kD dextrans (Fig. 5A and B), thus reminiscent of a reorganization of the FP and as

shown by the actin rearrangement upon DOX exposure (Fig. 5D). The latter may well have been the result of inhibited glycolysis, as was shown earlier to occur upon exposure of yeast [75] and HepG2 cells [76] exposed to DOX, possibly following binding of DOX to phosphofructokinase and α-enolase. Thus, DOX mediated inhibition of glycolysis should have resulted in early changes in the FP and thus also in the permeability of PODO/TERT256, as was observed under PhysOx, whereas DOX induced cell death [77] would be observed at higher concentrations. The fact that changes in permeability were observed under AtmOx at higher DOX concentrations only, corroborate the suggestion that podocytes cultures at AtmOx primarily generate ATP via OXPHOS, whereby cell death is then not induced via a reduced glycolysis but rather via apoptosis, necroptosis, ferroptosis etc. [77]. Consequently, use of PhysOx allowed to determine two important endpoints of DOX toxicity: i.) increased permeability and thus opening of the slit diaphragm at low DOX concentrations, and ii.) cell death at higher DOX concentrations.

In summary, PODO/TERT256 cells were demonstrated to be a robust and easy-to-handle cell line that expresses a wide variety of podocyte markers and displays podocyte-typical morphology. Furthermore, physiological oxygen (PhysOx) was shown to have a positive, physiologically enhancing effect on many of the parameters investigated e.g. the relocalization of Nephrin and P-Cadherin, two essential components of the slit diaphragm, and the sensitivity of the filtration barrier to DOX. Further incorporation of PODO/TERT256 in to a veritable human glomerulus *in vitro* system, would involve introduction of co-cultures and shear stress. Co-culturing cells has been demonstrated to improve the phenotype of a wide variety of cells [78–81]. Since the glomerular filtration barrier is formed by podocytes and endothelial cells a co-culture of PODO/TERT256 with glomerular microvascular endothelial cells appears to be critical for a reliable and veritable human glomerulus *in vitro* system. Finally, the incorporation of shear stress using a microfluidic system has already been shown to be beneficial for both ciPODs and podocytes differentiated from induced pluripotent stem cells [31,82]. Thus, co-culture of PODO/TERT256 and microvascular endothelial cells in a microfluidics setting with appropriate the oxygen tension and shear stress and in conjunction with functional endpoints, as presented here, could provide a solid basis for the development of more advanced *in vitro* renal testing systems that should be able to accurately predict nephrotoxicity in humans.

Declaration of competing interest

The authors declare the following financial interests/personal relationships which may be considered as potential competing interests: The authors declare no conflict of interest.

Daniel Dietrich reports financial support was provided by Boehringer Ingelheim Pharma GmbH & Co KG Biberach. Alexander Zielinski reports financial support was provided by KPK Invite. If there are other authors, they declare that they have no known competing financial interests or personal relationships that could have appeared to influence the work reported in this paper.

Data availability

No data was used for the research described in the article.

Acknowledgements

We thank the Bioimaging Center and the Electron Microscopy Center of the University of Konstanz for technical assistance and providing instrumentation. This project is supported by a collaborative research grant from Boehringer-Ingelheim Co KG Biberach an der Riß, Germany (#FP747/17) and the graduate training grant by KPK-InVite. Evercyte GmbH (Vienna, Austria) is acknowledged for providing the parental primary cells and its continuing collaboration.

Appendix A. Supplementary data

Supplementary data to this article can be found online at https://doi.org/10.1016/j.cbi.2023.110813.

References

[1] A. Greka, P. Mundel, Cell biology and pathology of podocytes, Annu. Rev. Physiol. 74 (2012) 299–323.
[2] H. Pavenstädt, W. Kriz, M. Kretzler, Cell biology of the glomerular podocyte, Physiol. Rev. 83 (2003) 253–307.
[3] F. Grahammer, C. Schell, T.B. Huber, The podocyte slit diaphragm—from a thin grey line to a complex signalling hub, Nat. Rev. Nephrol. 9 (2013) 587–598.
[4] M.R. Pollak, S.E. Quaggin, M.P. Hoenig, L.D. Dworkin, The glomerulus: the sphere of influence, Clin. J. Am. Soc. Nephrol. : CJASN 9 (2014) 1461–1469.
[5] R.P. Scott, S.E. Quaggin, The cell biology of renal filtration, JCB (J. Cell Biol.) 209 (2015) 199–210.
[6] J.B. Kopp, H.J. Anders, K. Susztak, M.A. Podesta, G. Remuzzi, F. Hildebrandt, P. Romagnani, Podocytopathies, Nat Rev Dis Primers 6 (2020) 68.
[7] A.J. Collins, R.N. Foley, D.T. Gilbertson, S.-C. Chen, United States Renal Data System public health surveillance of chronic kidney disease and end-stage renal disease, Kidney Int. Suppl. 5 (2015) 2–7.
[8] M. Abbate, C. Zoja, G. Remuzzi, How does proteinuria cause progressive renal damage? J. Am. Soc. Nephrol. 17 (2006) 2974–2984.
[9] J. Patrakka, K. Tryggvason, New insights into the role of podocytes in proteinuria, Nat. Rev. Nephrol. 5 (2009) 463–468.
[10] S.J. Shankland, The podocyte's response to injury: role in proteinuria and glomerulosclerosis, Kidney Int. 69 (2006) 2131–2147.
[11] W. Kriz, Progression of chronic renal failure in focal segmental glomerulosclerosis: consequence of podocyte damage or of tubulointerstitial fibrosis? Pediatr. Nephrol. 18 (2003) 617–622.
[12] S.E. Quaggin, J.A. Kreidberg, Development of the renal glomerulus: good neighbors and good fences, Development 135 (2008) 609–620.
[13] M.A. Saleem, One hundred ways to kill a podocyte, Nephrol. Dial. Transplant. 30 (2015) 1266–1271.
[14] K. Katsuya, E. Yaoita, Y. Yoshida, Y. Yamamoto, T. Yamamoto, An improved method for primary culture of rat podocytes, Kidney Int. 69 (2006) 2101–2106.
[15] J. Krtil, J. Platenik, M. Kazderova, V. Tesař, T. Zima, Culture methods of glomerular podocytes, Kidney Blood Press. Res. 30 (2007) 162–174.
[16] T. Sakairi, Y. Abe, H. Kajiyama, L.D. Bartlett, L.V. Howard, P.S. Jat, J.B. Kopp, Conditionally immortalized human podocyte cell lines established from urine, Am. J. Physiol. Ren. Physiol. 298 (2010) F557–F567.
[17] S.J. Shankland, J.W. Pippin, J. Reiser, P. Mundel, Podocytes in culture: past, present, and future, Kidney Int. 72 (2007) 26–36.
[18] M.A. Saleem, M.J. O'Hare, J. Reiser, R.J. Coward, C.D. Inward, T. Farren, C. Y. Xing, L. Ni, P.W. Mathieson, P. Mundel, A conditionally immortalized human podocyte cell line demonstrating nephrin and podocin expression, J. Am. Soc. Nephrol. 13 (2002) 630–638.
[19] L. Ni, M. Saleem, P.W. Mathieson, Podocyte culture: tricks of the trade, Nephrology 17 (2012) 525–531.
[20] D. Golosova, O. Palygin, R. Bohovyk, C.A. Klemens, V. Levchenko, D.R. Spires, E. Isaeva, A. El-Meanawy, A. Staruschenko, Role of Opioid Signaling in Kidney Damage during the Development of Salt-Induced Hypertension, vol. 3, Life Sci Alliance, 2020.
[21] A. Shalygin, L.S. Shuyskiy, R. Bohovyk, O. Palygin, A. Staruschenko, E. Kaznacheyeva, Cytoskeleton rearrangements modulate TRPC6 channel activity in podocytes, Int. J. Mol. Sci. 22 (2021).
[22] J. Tuffin, M. Chesor, V. Kuzmuk, T. Johnson, S.C. Satchell, G.I. Welsh, M. A. Saleem, GlomSpheres as a 3D co-culture spheroid model of the kidney glomerulus for rapid drug-screening, Commun. Biol. 4 (2021) 1351.
[23] T. Sakairi, Y. Abe, H. Kajiyama, L.D. Bartlett, L.V. Howard, P.S. Jat, J.B. Kopp, Conditionally immortalized human podocyte cell lines established from urine, Am. J. Physiol. Ren. Physiol. 298 (2010) F557–F567.
[24] V.C. Abraham, L.N. Miller, S.D. Pratt, B. Putman, L. Kim, S.M. Gopalakrishnan, A. King, Implementation of a human podocyte injury model of chronic kidney disease for profiling of renoprotective compounds, Eur. J. Pharmacol. 815 (2017) 219–232.
[25] S. Chittiprol, P. Chen, D. Petrovic-Djergovic, T. Eichler, R.F. Ransom, Marker expression, behaviors, and responses vary in different lines of conditionally immortalized cultured podocytes, Am. J. Physiol. Ren. Physiol. 301 (2011) F660–F671.
[26] H.W. Lee, S.Q. Khan, M.H. Faridi, C. Wei, N.J. Tardi, M.M. Altintas, H. A. Elshabrawy, S. Mangos, K.L. Quick, S. Sever, J. Reiser, V. Gupta, A podocyte-based automated screening assay identifies protective small molecules, J. Am. Soc. Nephrol. : JASN (J. Am. Soc. Nephrol.) 26 (2015) 2741–2752.
[27] T. May, D. Wirth, H. Hauser, P.P. Mueller, Transcriptionally regulated immortalization overcomes side effects of temperature-sensitive SV40 large T antigen, Biochem. Biophys. Res. Commun. 327 (2005) 734–741.
[28] J. Bejoy, J.M. Farry, J.L. Peek, M.C. Cabatu, F.M. Williams, R.C. Welch, E.S. Qian, L.E. Woodard, Podocytes derived from human induced pluripotent stem cells: characterization, comparison, and modeling of diabetic kidney disease, Stem Cell Res. Ther. 13 (2022) 355.

[29] J. Bejoy, E.S. Qian, L.E. Woodard, Accelerated protocol for the differentiation of podocytes from human pluripotent stem cells, STAR protocols 2 (2021), 100898-100898.

[30] O. Ciampi, R. Iacone, L. Longaretti, V. Benedetti, M. Graf, M.C. Magnone, C. Patsch, C. Xinaris, G. Remuzzi, A. Benigni, S. Tomasoni, Generation of functional podocytes from human induced pluripotent stem cells, Stem Cell Res. 17 (2016) 130–139.

[31] S. Musah, A. Mammoto, T.C. Ferrante, S.S.F. Jeanty, M. Hirano-Kobayashi, T. Mammoto, K. Roberts, S. Chung, R. Novak, M. Ingram, T. Fatanat-Didar, S. Koshy, J.C. Weaver, G.M. Church, D.E. Ingber, Mature induced-pluripotent-stem-cell-derived human podocytes reconstitute kidney glomerular-capillary-wall function on a chip, Nat. Biomed. Eng. 1 (2017).

[32] C. Rauch, E. Feifel, G. Kern, C. Murphy, F. Meier, W. Parson, M. Beilmann, P. Jennings, G. Gstraunthaler, A. Wilmes, Differentiation of human iPSCs into functional podocytes, PLoS One 13 (2018), e0203869.

[33] B. Song, A.M. Smink, C.V. Jones, J.M. Callaghan, S.D. Firth, C.A. Bernard, A. L. Laslett, P.G. Kerr, S.D. Ricardo, The directed differentiation of human iPS cells into kidney podocytes, PLoS One 7 (2012), e46453.

[34] M. Leist, T. Hartung, Inflammatory findings on species extrapolations: humans are definitely no 70-kg mice, Arch. Toxicol. 87 (2013) 563–567.

[35] H. Olson, G. Betton, D. Robinson, K. Thomas, A. Monro, G. Kolaja, P. Lilly, J. Sanders, G. Sipes, W. Bracken, M. Dorato, K. Van Deun, P. Smith, B. Berger, A. Heller, Concordance of the toxicity of pharmaceuticals in humans and in animals, Regul. Toxicol. Pharmacol. 32 (2000) 56–67.

[36] J.M. McKim Jr., Building a tiered approach to in vitro predictive toxicity screening: a focus on assays with in vivo relevance, Combinatorial chemistry & high throughput screening 13 (2010) 188–206.

[37] J.Y.C. Soo, J. Jansen, R. Masereeuw, M.H. Little, Advances in predictive in vitro models of drug-induced nephrotoxicity, Nat. Rev. Nephrol. 14 (2018) 378–393.

[38] C.E. Nestor, R. Ottaviano, D. Reinhardt, H.A. Cruickshanks, H.K. Mjoseng, R. C. McPherson, A. Lentini, J.P. Thomson, D.S. Dunican, S. Pennings, S.M. Anderton, M. Benson, R.R. Meehan, Rapid reprogramming of epigenetic and transcriptional profiles in mammalian culture systems, Genome Biol. 16 (2015) 11.

[39] L.J. Hale, S.E. Howden, B. Phipson, A. Lonsdale, P.X. Er, I. Ghobrial, S. Hosawi, S. Wilson, K.T. Lawlor, S. Khan, A. Oshlack, C. Quinlan, R. Lennon, M.H. Little, 3D organoid-derived human glomeruli for personalised podocyte disease modelling and drug screening, Nat. Commun. 9 (2018) 5167.

[40] P.F. Secker, L. Lisanne, N. Schlichenmaier, D.R. Dietrich, RPTEC/TERT1 cells form highly differentiated tubules when cultured in a 3D matrix, ALTEX 35 (2018) 223–234.

[41] S.Y. Zhang, G.J. Mahler, Modelling renal filtration and reabsorption processes in a human glomerulus and proximal tubule microphysiological system, Micromachines 12 (2021).

[42] M. Muller, W. Padberg, E. Schindler, J. Sticher, C. Osmer, S. Friemann, G. Hempelmann, Renocortical tissue oxygen pressure measurements in patients undergoing living donor kidney transplantation, Anesth. Analg. 87 (1998) 474–476.

[43] W. Neuhofer, F.-X. Beck, Cell survival in the hostile environment of the renal medulla, Annu. Rev. Physiol. 67 (2005) 531–555.

[44] A. Carreau, B.E. Hafny-Rahbi, A. Matejuk, C. Grillon, C. Kieda, Why is the partial oxygen pressure of human tissues a crucial parameter? Small molecules and hypoxia, J. Cell Mol. Med. 15 (2011) 1239–1253.

[45] C. Mas-Bargues, J. Sanz-Ros, A. Román-Domínguez, M. Inglés, L. Gimeno-Mallench, M. El Alami, J. Viña-Almunia, J. Gambini, J. Viña, C. Borrás, Relevance of oxygen concentration in stem cell culture for regenerative medicine, Int. J. Mol. Sci. 20 (2019).

[46] L. Jagannathan, S. Cuddapah, M. Costa, Oxidative stress under ambient and physiological oxygen tension in tissue culture, Curr Pharmacol Rep 2 (2016) 64–72.

[47] B. Halliwell, Cell culture, oxidative stress, and antioxidants: avoiding pitfalls, Biomed. J. 37 (2014) 99–105.

[48] J.A. Stuart, J. Fonseca, F. Moradi, C. Cunningham, B. Seliman, C.R. Worsfold, S. Dolan, J. Abando, L.A. Maddalena, How supraphysiological oxygen levels in standard cell culture affect oxygen-consuming reactions, Oxid. Med. Cell. Longev. 2018 (2018) 13.

[49] W. Xiao, M. Shinohara, K. Komori, Y. Sakai, H. Matsui, T. Osada, The importance of physiological oxygen concentrations in the sandwich cultures of rat hepatocytes on gas-permeable membranes, Biotechnol. Prog. 30 (2014) 1401–1410.

[50] K.M. Lee, K.H. Choi, M.M. Ouellette, Use of exogenous hTERT to immortalize primary human cells, Cytotechnology 45 (2004) 33–38.

[51] S. Schildknecht, D. Poltl, D.M. Nagel, F. Matt, D. Scholz, J. Lotharius, N. Schmieg, A. Salvo-Vargas, M. Leist, Requirement of a dopaminergic neuronal phenotype for toxicity of low concentrations of 1-methyl-4-phenylpyridinium to human cells, Toxicol. Appl. Pharmacol. 241 (2009) 23–35.

[52] M.J. Karnovsky, A formaldehyde-glutaraldehyde fixative of high osmolality for use in electron-microscopy, JCB (J. Cell Biol.) 27 (1965) 137.

[53] N. Chaffey, M.A. Hayat, Principles and Techniques of Electron Microscopy: Biological Applications, fourth ed., 2000, p. 543. Cambridge: Cambridge University Press. £65 (hardback), Annals of Botany, 87 (2001) 546-548.

[54] M.D. Abràmoff, P.J. Magalhães, S.J. Ram, Image processing with ImageJ, Biophot. Int. 11 (2004) 36–42.

[55] A. Limonciel, L. Aschauer, A. Wilmes, S. Prajczer, M.O. Leonard, W. Pfaller, P. Jennings, Lactate is an ideal non-invasive marker for evaluating temporal alterations in cell stress and toxicity in repeat dose testing regimes, Toxicol. Vitro 25 (2011) 1855–1862.

[56] B. Srinivasan, A.R. Kolli, M.B. Esch, H.E. Abaci, M.L. Shuler, J.J. Hickman, TEER measurement techniques for in vitro barrier model systems, J. Lab. Autom. 20 (2015) 107–126.

[57] P.K. Mattila, P. Lappalainen, Filopodia: molecular architecture and cellular functions, Nat. Rev. Mol. Cell Biol. 9 (2008) 446–454.

[58] C. Faul, K. Asanuma, E. Yanagida-Asanuma, K. Kim, P. Mundel, Actin up: regulation of podocyte structure and function by components of the actin cytoskeleton, Trends Cell Biol. 17 (2007) 428–437.

[59] J.K. Guo, A.L. Menke, M.C. Gubler, A.R. Clarke, D. Harrison, A. Hammes, N. D. Hastie, A. Schedl, WT1 is a key regulator of podocyte function: reduced expression levels cause crescentic glomerulonephritis and mesangial sclerosis, Hum. Mol. Genet. 11 (2002) 651–659.

[60] J. Reiser, W. Kriz, M. Kretzler, P. Mundel, The glomerular slit diaphragm is a modified adherens junction, J. Am. Soc. Nephrol. 11 (2000) 1–8.

[61] M. Sanchez-Niño, M. Pérez Gómez, L. Valiño, R. Torra, A. Ortiz, Podocyturia: why it may have added value in rare diseases, Clinical Kidney Journal 12 (2018).

[62] J. Reiser, M.M. Altintas, Podocytes F1000Res (2016) 5.

[63] P.F. Secker, N. Schlichenmaier, M. Beilmann, U. Deschl, D.R. Dietrich, Functional Transepithelial Transport Measurements to Detect Nephrotoxicity in Vitro Using the RPTEC/TERT1 Cell Line, Archives of Toxicology, 2019.

[64] O. Delézay, Z. He, S. Hodin, M.A. Saleem, P. Mismetti, N. Perek, X. Delavenne, Glomerular filtration drug injury: in vitro evaluation of functional and morphological podocyte perturbations, Exp. Cell Res. 361 (2017) 300–307.

[65] H. Liu, X. Gao, H. Xu, C. Feng, X. Kuang, Z. Li, X. Zha, α-Actinin-4 is involved in the process by which dexamethasone protects actin cytoskeleton stabilization from adriamycin-induced podocyte injury, Nephrology 17 (2012) 669–675.

[66] P.K.-T. Li, T.K.-W. Ma, Global impact of nephropathies, Nephrology 22 (2017) 9–13.

[67] C.D. Mathers, D. Loncar, Projections of global mortality and burden of disease from 2002 to 2030, PLoS Med. 3 (2006) e442.

[68] R.A. Nugent, S.F. Fathima, A.B. Feigl, D. Chyung, The burden of chronic kidney disease on developing nations: a 21st century challenge in global health, Nephron Clin. Pract. 118 (2011) c269–c277.

[69] N. Sanchez-Romero, C.M. Schophuizen, I. Gimenez, R. Masereeuw, In vitro systems to study nephropharmacology: 2D versus 3D models, Eur. J. Pharmacol. 790 (2016) 36–45.

[70] A. Krebs, T. Waldmann, M.F. Wilks, B.M.A. Van Vugt-Lussenburg, B. Van der Burg, A. Terron, T. Steger-Hartmann, J. Ruegg, C. Rovida, E. Pedersen, G. Pallocca, M. Luijten, S.B. Leite, S. Kustermann, H. Kamp, J. Hoeng, P. Hewitt, M. Herzler, J. G. Hengstler, T. Heinonen, T. Hartung, B. Hardy, F. Gantner, E. Fritsche, K. Fant, J. Ezendam, T. Exner, T. Dunkern, D.R. Dietrich, S. Coecke, F. Busquet, A. Braeuning, O. Bondarenko, S.H. Bennekou, M. Beilmann, M. Leist, Template for the description of cell-based toxicological test methods to allow evaluation and regulatory use of the data, ALTEX 36 (2019) 682–699.

[71] K.E. Haley, N.M. Kronenberg, P. Liehm, M. Elshani, C. Bell, D.J. Harrison, M. C. Gather, P.A. Reynolds, Podocyte injury elicits loss and recovery of cellular forces, Sci. Adv. 4 (2018), eaap8030.

[72] L.H. Lash, Diverse roles of mitochondria in renal injury from environmental toxicants and therapeutic drugs, Int. J. Mol. Sci. 22 (2021) 4172.

[73] P.T. Brinkkoetter, T. Bork, S. Salou, W. Liang, A. Mizi, C. Özel, S. Koehler, H. H. Hagmann, C. Ising, A. Kuczkowski, S. Schnyder, A. Abed, B. Schermer, T. Benzing, O. Kretz, V.G. Puelles, S. Lagies, M. Schlimpert, B. Kammerer, C. Handschin, C. Schell, T.B. Huber, Anaerobic glycolysis maintains the glomerular filtration barrier independent of mitochondrial metabolism and dynamics, Cell Rep. 27 (2019) 1551–1566.e1555.

[74] S. Ozawa, S. Ueda, H. Imamura, K. Mori, K. Asanuma, M. Yanagita, T. Nakagawa, Glycolysis, but not Mitochondria, responsible for intracellular ATP distribution in cortical area of podocytes, Sci. Rep. 5 (2015), 18575-18575.

[75] H. Taymaz-Nikerel, M.E. Karabekmez, S. Eraslan, B. Kirdar, Doxorubicin induces an extensive transcriptional and metabolic rewiring in yeast cells, Sci. Rep. 8 (2018), 13672.

[76] A. Korga, M. Ostrowska, M. Iwan, M. Herbet, J. Dudka, Inhibition of glycolysis disrupts cellular antioxidant defense and sensitizes HepG2 cells to doxorubicin treatment, FEBS Open Bio 9 (2019) 959–972.

[77] E. Christidi, L.R. Brunham, Regulated cell death pathways in doxorubicin-induced cardiotoxicity, Cell Death Dis. 12 (2021) 339.

[78] M. Li, A. Corbelli, S. Watanabe, S. Armelloni, M. Ikehata, V. Parazzi, C. Pignatari, L. Giardino, D. Mattinzoli, L. Lazzari, A. Puliti, F. Cellesi, C. Zennaro, P. Messa, M. P. Rastaldi, Three-dimensional podocyte–endothelial cell co-cultures: assembly, validation, and application to drug testing and intercellular signaling studies, Eur. J. Pharmaceut. Sci. 86 (2016) 1–12.

[79] F. Tasnim, D. Zink, Cross talk between primary human renal tubular cells and endothelial cells in cocultures, Am. J. Physiol. Ren. Physiol. 302 (2012) F1055–F1062.

[80] J.P. Waters, Y.C. Richards, J.N. Skepper, M. Southwood, P.D. Upton, N.W. Morrell, J.S. Pober, J.R. Bradley, A 3D tri-culture system reveals that activin receptor-like kinase 5 and connective tissue growth factor drive human glomerulosclerosis, J. Pathol. 243 (2017) 390–400.

[81] F. Piossek, S. Beneke, N. Schlichenmaier, G. Mucic, S. Drewitz, D.R. Dietrich, Physiological oxygen and co-culture with human fibroblasts facilitate in vivo-like properties in human renal proximal tubular epithelial cells, Chem. Biol. Interact. 361 (2022), 109959.

[82] M. Zhou, X. Zhang, X. Wen, T. Wu, W. Wang, M. Yang, J. Wang, M. Fang, B. Lin, H. Lin, Development of a functional glomerulus at the organ level on a chip to mimic hypertensive nephropathy, Sci. Rep. 6 (2016), 31771.